Inhomogeneous contraction of interatomic distances in metallic clusters: Calculations for Cs_n and OCs_n

A. Mañanes
Departamento de Física Moderna, Universidad de Cantabria, E-39005 Santander, Spain

J. A. Alonso
Departamento de Física Teórica, Universidad de Valladolid, E-47005 Valladolid, Spain

U. Lammers and G. Borstel
Fachbereich Physik, Universität Osnabrück, D-4500 Osnabrück, Germany
(Received 11 March 1991)

The equilibrium geometrical structures of Cs_n and OCs_n clusters have been obtained by a method that, in the framework of density-functional theory, describes the ion-electron interaction by means of a pseudopotential that is spherically averaged about the cluster center. In the size range studied (up to $n=78$ and 70, respectively) the clusters present well-separated atomic layers for which the distances to the two closest neighbors of each atom have been analyzed, showing that there is an inhomogeneous shrinking of the geometrical structure, in the sense that the distances obtained for atoms in the inner layers are lower than those for the outer ones. The analysis of the growing of the clusters suggests that the equilibrium geometries are those for which any atom of the aggregate has its closest neighbor at a distance lower than the nearest-neighbor distance of the pure bulk metal. For small ($n \leq 20$) pure clusters, geometries of high symmetry have been found, which are completely modified by the presence of the oxygen impurity. A regular octahedron is formed around the oxygen atom in most cases.

I. INTRODUCTION

Metallic clusters are remarkable examples of finite quantum systems. The size dependence of some of their properties, for example, the abundance spectra and the ionization potentials (IP), is well understood, for the case of simple metallic elements, in the framework of the jellium model,[1,2] which is an extension of the free-electron model of bulk metals. In the case of clusters, the quantum states of the valence electrons are determined by the self-consistent mean field produced by the finite positive ionic distribution, considered as continuous (jellium model), and the electron-electron interaction. For clusters with number of atoms n smaller than 100, the assumption of a homogeneous spherical jellium distribution allows the reproduction of experimentally found local maxima in the abundances, magic numbers, which coincide with those clusters with completely filled electronic shells and with the next empty shell well separated in energy.[3,4] The corresponding ionization potentials present a steplike behavior when we pass from the magic cluster n to its neighbor $n+1$, in agreement with experiment, although the calculated drops are, in general, greater than the measured ones.[5] Several refinements of this self-consistent spherical model have been proposed, such as the inclusion of spheroidal distortions[6] and the use of diffuse positive distributions.[7]

Recently, experimental results on the abundances have been obtained by Martin and co-workers for large clusters of OCs_n, with $n \leq 600$ (Ref. 8) and Na_n, with $n \leq 1500$ (Refs. 9 and 10), which have been explained by means of an inhomogeneous jellium model. A positive density that is higher than the bulk average value is needed at the center of the cluster in order to produce the bunching of the electronic levels necessary to give the right sequence of magic numbers. Martin and co-workers found it impossible to predict the experimental values of the most abundant clusters, for $n \geq 100$, with a homogeneous distribution, although both distributions give the same sequence for the light clusters, $n \leq 100$. The calculated ionization potentials for the centrally compressed spherical background present also steps at those magic numbers observed experimentally for large clusters and a reduction of step size in the IP values for light clusters, $n \leq 100$.[10]

In this contribution we present an analysis of the equilibrium geometries obtained for Cs_n with $3 \leq n \leq 78$ and OCs_n, $3 \leq n \leq 70$, using a model that, in the framework of density functional theory, includes also the ionic structure of the aggregate, transcending the jellium model but retaining the spherical assumption for the external potential. The ion-electron interaction for the valence electrons is thus approximated by the spherical average of the pseudopotential (SAPS method[11]). Some results concerning the cohesive energies, electronic structure, ionization potentials, embedding energy of the oxygen atom, and general geometrical trends have already been published.[12,13] We have compared the IP's for OCs_n with the experimental values, showing that the SAPS scheme reproduces the general trend and the drop after a magic number, those drops greater than the experimental ones.[12] The inadequacy of the homogeneous jellium model to describe the expected sequence of magic numbers of Cs_n was discussed in Ref. 13, where we have shown that

the inclusion of the ionic structure gives the expected sequence for pure clusters (expected from trends in the measured ionization potential[14]) and the experimental one for suboxide OCs_n clusters.[15] In the present work we analyze the ion-ion distances in the clusters and the detailed geometrical structure showing that an inhomogeneous shrinking is obtained from our calculations in agreement with the conclusions of T. P. Martin's group.[8,9] Also, a recent SAPS calculation[16] for aluminum clusters Al_n, $3 \leq n \leq 25$, explains the deviations of the predicted values of the polarizability within the homogeneous jellium model from the experimental results as due to the actual contraction of the small Al_n clusters. Finally, we point out that lattice contractions have been measured in Au and Pt clusters,[17] and also that a size-dependent contraction of the nearest-neighbor distances for clusters isolated in solid argon has been measured for Ag and Cu clusters,[18,19] thus indicating that the effect could be a general property of any metallic cluster.

II. THE MODEL

The model used to calculate the electronic and geometrical structures of the clusters has been presented in detail elsewhere[11–13,20] and we stress here only the main points. For an initial geometry of the cluster, the Kohn-Sham equations of density-functional theory[21] are self-consistently solved, using the local-density approximation for the exchange-correlation energy. Afterward the ionic coordinates are moved, with a steepest-descent method and preserving the self-consistency between the ionic positions and the electronic density, to obtain the equilibrium geometry and the corresponding ground-state total energy E. To avoid trapping in a local minimum several initial random geometries are considered (40 for pure clusters and 70 for the OCs_n). An empty-core pseudopotential is used to describe the ion-electron interaction with a core radius, $r_c(\mathrm{Cs}) = 2.74$ a.u., which leads to the experimental ionization potential in the free-atom limit for the same density functional method. The total ionic potential of the cluster is spherically averaged around the center of mass of the cluster. This is equivalent to using the spherically averaged electronic density in the calculations and it is the most drastic approximation of our model which must be more accurate the bigger the cluster becomes. However, the exact ion-ion repulsion is included in the calculations, which makes the total energy a function of the precise location of the atoms. For OCs_n all the electrons of the oxygen atom are considered in the calculation and the positive nuclear charge is always located at the center of mass of the cluster reinforcing the spherical symmetry assumed for the aggregate.

The results of our calculations[12,13] reproduce the electronic shell effects associated with the local maxima in the abundance spectrum of OCs_n. The sequence of single-electron shells obtained $(1s, 2s, 1p, 3s, 2p, 1d, 1f, 4s, 3p, 1g, 2d)$ produces, once the electronic configuration of the ion O^{2-} $(1s^2 2s^2 1p^6)$ is considered, the following closing-shell numbers: $n = 4, 10, 20, 34, 36, 42, 60$. When the near degeneracy of the $4s$-$1f$ and $1g$-$3p$ shells is taken into account, the relative high stability of clusters with

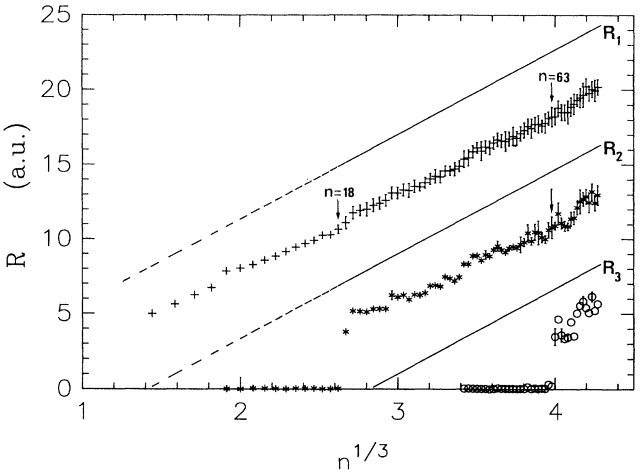

FIG. 1. Mean radius and standard deviation as functions of $n^{1/3}$ for the atomic layers of Cs_n clusters. The straight lines, R_i, given by Eq. (1), separate the three regions defined in the clusters. R_1 corresponds to the radius of the homogeneous spherical jellium. The vertical arrows indicate the largest clusters with a central atom and one and two atomic layers, respectively.

$n = 10, 20, 36$, and 60 due to electronic effects arises from the SAPS calculations, in agreement with the experimental results.[15] For pure Cs clusters the sequence obtained $(1s, 1p, 1d, 2s, 1f, 2p, 1g, 2d, 3s, 1h)$ presents three shells nearly degenerate in energy ($2d$, $3s$, and $1h$), so the following sequence of magic numbers was predicted: $n = 8$, 18, 20, 34, 40, and 58, in accordance with the results for other alkali-metal clusters.[2]

III. THE GROWING OF THE CLUSTERS

The main trends of the geometrical structures of Cs_n and OCs_n are summarized in Figs. 1 and 2, respectively.

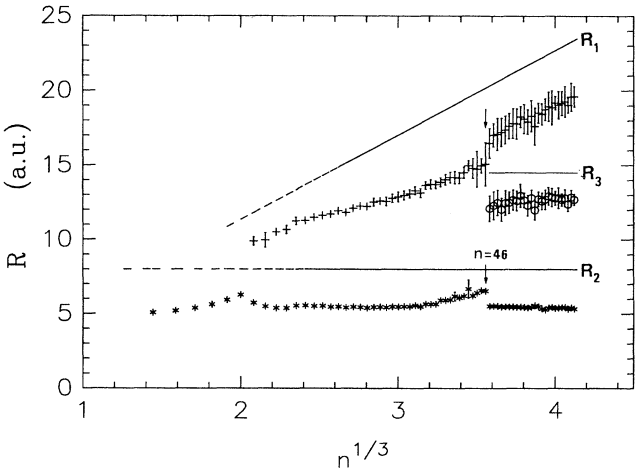

FIG. 2. The same quantities as in Fig. 1 now for the Cs atoms in OCs_n clusters. The oxygen atom is in the cluster center. The vertical arrow indicates the biggest cluster with only two atomic shells.

The atoms are arranged in spherical layers around the cluster center; these layers are clearly separated in the radial direction and the atoms within each one show a small relative dispersion in the radial coordinate. The mean radius of each atomic shell and the standard deviations are given in the figures. The corresponding number of atoms in each layer has been given in Figs. 4 and 9 of Ref. 13. The radial distribution of the ions and the electronic densities are given in Fig. 3 for some selected clusters, Cs_{20}, OCs_{20}, Cs_{60}, and OCs_{60}, of which the first three have closed electronic shells (the actual geometry obtained for Cs_{20} will be given in Fig. 8). The atomic layering is clearly shown and also the corresponding correlation with the oscillations in the electronic density. It is also remarkable that the presence of the oxygen impurity produces only a small modification of the outer maximum of the electronic density, which is located at $r \simeq 9$ a.u. for $n=20$ and at $r \simeq 14-15$ a.u. for $n=60$. This indicates that the atomic layer surrounding the oxygen atom produces a very strong screening of the impurity and consequently its effect on the outer part of the cluster becomes less noticeable. The screening effect is even more notorious for those clusters which have nearly identical radial distributions of the Cs atoms in the pure and in the OCs_n cases. Such is the case for $26 \leq n \leq 32$ (with the only exception of $n=29$), a group of aggregates which, in the pure case, have no central atom and an inner shell of six Cs atoms (only five for $n=29$), the same radial distribution as the one obtained for the corresponding OCs_n. For these clusters, a minimum value of the calculated embedding energy $\Delta H(n) \equiv E(OCs_n) - E(Cs_n) - E(O)$ of oxygen in Cs_n is obtained, as was discussed in Ref. 13. In Fig. 4 two pairs of aggregates are given for comparison: Cs_{26}, OCs_{26} and Cs_{32}, OCs_{32}. The oxygen produces a very small change in the electronic density of the outer part of the clusters ($r \geq 5$ a.u.) and a small shrinking of the ionic distributions in the radial direction. This last effect is more noticeable for the internal shell of six atoms, as the outer part of the cluster only slightly modified because of the strong screening produced by the innermost shell. In the region of larger sizes an analogous situation is expected for Cs_{73} and Cs_{76}: The radial distributions of these clusters show an inner shell of six atoms and a vacancy at the central site. However, we have not extended our calculations to those sizes for OCs_n and we do not have the corresponding data to be compared. The strong ionic bonding of the oxygen is also responsible for the large shrinking obtained for Cs_6 (an octahedron with an edge of 9.5 a.u.) when the impurity is embedded: OCs_6 is also an octahedron, with the oxygen at its center, but now the value of the edge is 7.96 a.u. For those OCs_n aggregates whose internal geometry is also that of OCs_6, the value of the edge oscillates between 7.7 and 7.8 a.u. These results contrast with the expansion of the geometrical structure when a Cs atom is located at the center: Cs_7 is a centered octahedron with an edge of 11.1 a.u.

For pure cesium the population of each atomic layer increases with the total number of atoms and the cluster strongly reconstructs as it grows. The growth can be de-

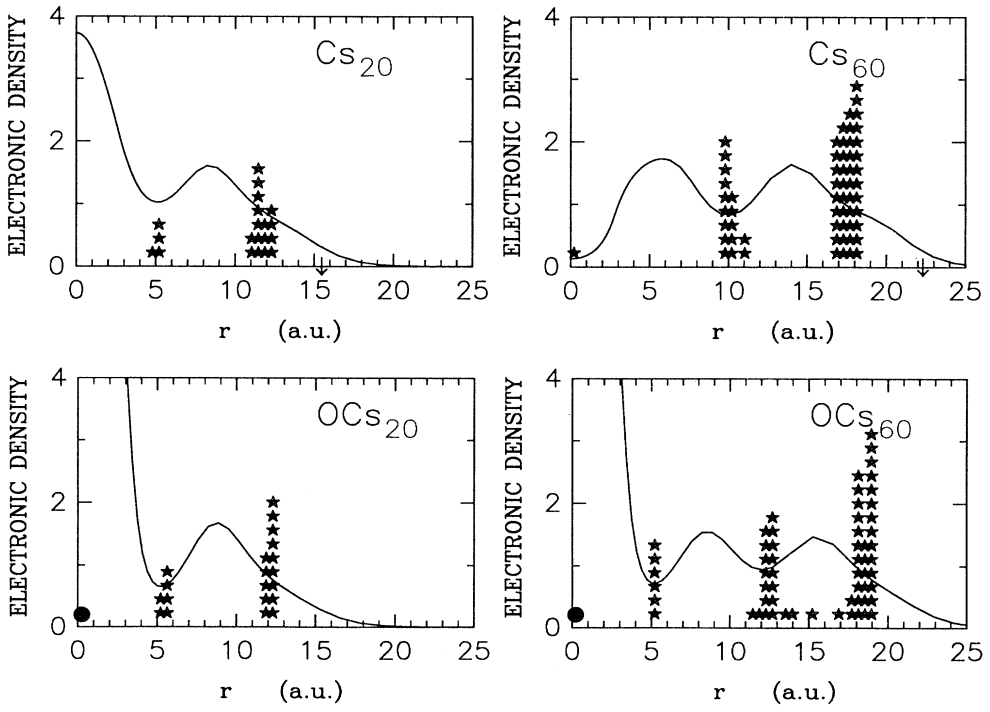

FIG. 3. Radial distribution of the atoms and electronic densities for Cs_{20}, OCs_{20}, Cs_{60}, and OCs_{60}. The units for the electronic density are $n_0 = 1/\Omega(Cs)$, where $\Omega(Cs)$ is the volume per atom in the pure bulk metal. The stars indicate Cs atoms and the circle the oxygen. The vertical arrow in the plots for pure Cs clusters indicates the homogeneous jellium radius $R = r_s n^{1/3}$.

scribed such that new shells appear in the innermost region of the cluster when certain conditions are met. This can be appreciated in Fig. 1, where we have indicated with two vertical arrows the biggest clusters with one central atom and one and two additional atomic layers, Cs_{18} and Cs_{63}, respectively. For Cs_{18} the distance between the central atom and any atom in the surface layer becomes slightly larger than the nearest-neighbor distance in bulk Cs, $d_{NN}=9.893$ a.u. Our calculation indicates that the cluster Cs_{19} reconstructs its geometry in such a way as to avoid neighbor interatomic distances larger than d_{NN}. This is achieved by locating the added atom in the interior of the cluster (see the geometrical structures obtained for Cs_{18} and Cs_{19} in Fig. 7) instead of placing it on the surface, a situation which would have increased the cluster radius (and distances between neighbors) further. For Cs_{63} the situation is analogous to that of Cs_{18}. Now the central atom is surrounded by an atomic shell of 19 atoms at a mean radius nearly identical to that of Cs_{18} and again clearly larger than d_{NN}. The next cluster, Cs_{64}, has two atoms in the inner region, like Cs_{19}, forming a new shell that is populated as the cluster grows in size. This behavior is again an indication that neighbor interatomic distances greater than d_{NN} are avoided in the equilibrium geometries of the clusters.

In the case of OCs_n a stable inner structure, typically of six atoms arranged as a regular octahedron, is formed around the oxygen impurity for any cluster size.[13] This means that, in general, the geometrical structure of Cs_n is strongly perturbed by the presence of the oxygen, as a comparison of Cs_{60} and OCs_{60} in Fig. 3 clearly shows. For these suboxide clusters the growth pattern differs from that in pure Cs. An intermediate Cs shell appears at OCs_{47} midway between the surface shell and the inner core. The appearance of this new atomic shell can be explained by the same argument as in the case of pure Cs: From Fig. 2 the values of the radii of the two atomic shells of OCs_{46} are 6.5 a.u. and 15 ± 1.5 a.u., respectively, and this means that the minimum distance between a Cs atom in the inner part and another in the outer part is of the order of, or greater than, d_{NN}, because two atoms in different shells are never in the same radial direction (in this cluster); if it is assumed that no Cs atom in any finite aggregate can be located at a distance from all the other atoms that is clearly greater than d_{NN}, as the results for pure Cs suggest, a new intermediate shell should form in order to fulfill this condition. This intermediate layer bridges the two parts of the OCs_n clusters and makes the radius of the surface layer increase faster (see Fig. 2). The number of atoms in the intermediate layer increases from 13 to 22 between OCs_{47} and OCs_{70}, although with an oscillatory behavior. However, the corresponding shell radius is rather stable. In fact, for $60\leq n\leq 70$ the number of atoms in this layer oscillates only between 19 and 22 with a more stable value for the radius also.

IV. THE INHOMOGENEOUS CONTRACTION

In order to show the inhomogeneous shrinking of the interatomic distances of the clusters we have divided each

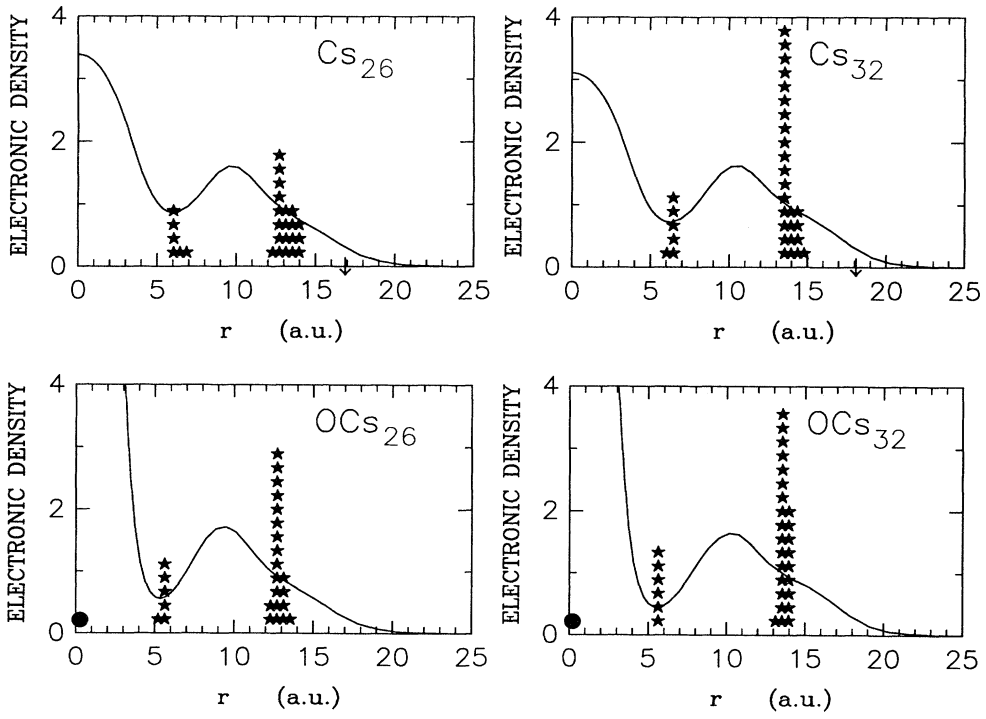

FIG. 4. Radial distribution of the atoms and electronic densities for Cs_{26}, OCs_{26}, Cs_{32}, and OCs_{32}. Symbols and units are as in Fig. 3.

aggregate in several regions, each one including only one atomic shell, which are separated by the radii indicated by the straight lines in Figs. 1 and 2. For each atom within one of those regions we look for the two closest ions at any point in the cluster and not only inside its own atomic shell. Finally, the mean value of the distances to the nearest atom D_1 and of the distances to the two nearest atoms D_2 are obtained for the collection of atoms within the chosen regions. The regions considered are separated by the radii given by the following relationship:

$$R_i(n)=a_i+b_i n^{1/3}\ , \quad i=1,2,3\ , \tag{1}$$

where, for Cs_n, $b_1=b_2=b_3=r_s$ (r_s is the Wigner-Seitz radius for bulk cesium, $r_s=5.67$ a.u.), $a_1=0$, $a_2=-8.0$ a.u., $a_3=-16.0$ a.u., and only the positive values of $R_i(n)$ are considered. These radii clearly separate the atomic shells that actually exist in the Cs aggregates. Actually, only two radii are necessary to separate the three regions considered. The most external radius, $R_1=r_s n^{1/3}$, which is the radius of a cluster of n atoms in the spherical jellium model, is included only to illustrate the global contraction of the cluster volume with respect to a piece of the macroscopic metal with the same number of atoms. For OCs_n the three regions considered correspond to the following values of the coefficients in (1): $b_1=r_s$, $b_2=b_3=0$, and $a_1=0$, $a_2=8.5$ a.u., $a_3=15.0$ a.u.; in this case only two regions are considered for $9\le n\le 45$, and three regions are analyzed for $46\le n\le 70$. The results for the mean values and the standard deviations for the distances to the closest atom D_1 and to the two closest atoms D_2 are given in Figs. 5 and 6 for Cs_n and OCs_n, respectively. Also the experimental value of the nearest-neighbor distance for bulk cesium, d_{NN}, is given for comparison.

At this point it is important to notice that the two closest atoms (of a given one) mentioned here have not the same meaning as the nearest-neighbor and second-nearest-neighbor for a perfect crystal in solid state physics. As we show in the following, the interatomic distances for a Cs cluster are not as well defined as in a perfect crystal (that is, there is a larger dispersion). By means of D_1 and D_2 we are trying to obtain the average nearest-neighbor distance for atoms in the different regions defined above. Actually, an average over a larger number of closest atoms, D_3, D_4, etc., may be better. Ideally one should average over the first coordination shell, but the problem is that its population around an inner atom is different from that for a surface atom. To avoid these additional complications we stop with D_2, since we consider that it is enough for our purposes.

A. Cs_n clusters

In the case of Cs_n Fig. 5(a) shows that atoms in the inner parts of the cluster have their first neighbor closer than those atoms that are in the outer parts of the aggregate. The behavior of D_1 in the two zones $7\le n\le 18$ and $40\le n\le 63$ is due to the singular character of the central atom in these clusters. In the first zone there is only one atomic shell plus one atom at the center, and Fig. 5(a) shows that for $7\le n\le 13$ the closest atom to any one in the external shell is the central atom and vice versa, so the lines for D_1 corresponding to the outer shell (crosses) and to the central atom (stars) are practically identical. However, from Cs_{14} to Cs_{18} the atom closest to one in the surface is also on the surface at a distance which is lower than the mean radius of the atomic layer. Now the line corresponding to the central atom is clearly over the mean value D_1 for the external shell. The sudden drop in the value of D_1 at Cs_{19} is due to the formation of the new internal shell already described. For Cs_{18} the value of D_1 corresponding to the central atom is slightly larger than d_{NN} (see arrow in the figure), so the transition reflects the fact that the preferred equilibrium geometry is one in which the values of D_1 for any region of the cluster are always lower than d_{NN}, as is the case for Cs_{19}.

A similar behavior is obtained for D_1 in the range $40\le n\le 63$ in which there is also only one atom (the central one) in the innermost region defined by the radius R_3. For this region, D_1 increases with the cluster size, associated with the corresponding increment of the radius of the intermediate shell, and a sudden decrease occurs when a new inner shell of two atoms is formed at Cs_{64}. However, in this size range the values of D_1 for the

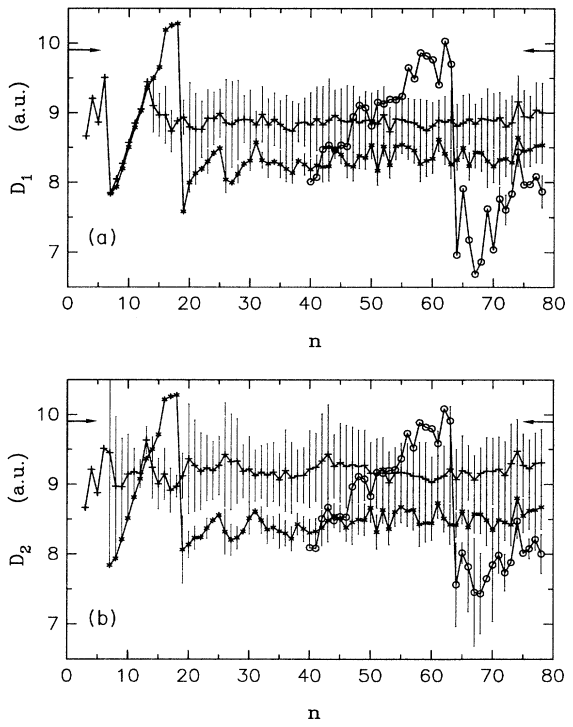

FIG. 5. (a) Mean distance to the nearest Cs atom and standard deviation, for the three regions defined in Fig. 1 for Cs_n clusters, as a function of n. (b) Mean values of the distances to the two nearest Cs atoms for each of the regions. In both cases the horizontal arrow corresponds to the nearest-neighbor distance in pure bulk cesium, $d_{NN}=9.893$ a.u.

intermediate shell are lower (only in three cases are slightly larger) than those for the central atom. This is due to the contraction of this shell with respect to the case of single layered clusters, as can be shown when its population is considered. The number of atoms in this intermediate shell is 10 (for $n=40$, 41, and 44) and 12 (for $n=42$, 43, 45, 46, and 50). The values of D_1 for the central atom are, in both cases, clearly lower than those corresponding to the central atom of Cs_{11} and Cs_{13}, respectively. The contraction is about 0.8 a.u. for most of the clusters considered. Also the values of D_1 corresponding to the intermediate layer are lower than those corresponding to the outer part of the single layered clusters, Cs_{11} and Cs_{13}, indicating that these intermediate layers are more closely packed. When the population in this intermediate shell is greater than 12, the corresponding values of D_1 for the two regions defined by R_2 and R_3 are clearly different, showing that for these clusters the closest atom to one in the intermediate shell is never the central one. A maximum value of 19 atoms surrounding the central one is reached at Cs_{63}, with a radius for the spherical shell of the order of d_{NN} like in the case of Cs_{18}, thus promoting the formation of a new internal shell for the larger clusters.

The values of D_1, and also of D_2 in Fig. 5(b), are fairly constant in the range studied except at the first steps of the formation of a new shell, for example, the most internal shell, for $64 \leq n \leq 78$, which only has a number of atoms between 2 and 6. The oscillation in D_1 for the external shell of the light clusters, when $n \leq 13$, is smoothed by the inclusion of the distance to the second closest atom in D_2, Fig. 5(b), with the corresponding increment in the standard deviations. The reason is that for $7 \leq n \leq 13$ the closest distance between atoms in the outer shell is, as mentioned above, bigger than the mean radius of the shell, being Cs_{13}, a centered icosahedron, the first cluster for which both distances are similar.

In Fig. 5(b) the values of D_2 also show the same effect of inhomogeneous contraction of the clusters. For those aggregates with a central atom, D_2 coincides with D_1 for the region that only contains the central atom due to the spherical arrangement of the layer surrounding the center of the cluster. It is important to point out that if the central atom had been included as part of its closest shell for the calculation of D_1 and D_2, the values obtained should not be very different from those quoted because of the small relative influence of one distance (with the value given in the figures) in the mean values of 7–19 (the populations of the shell closest to the central atom) distances. Actually, we feel that defining a region with only one atom is not satisfactory, as shown by the peculiar behavior of this region in Fig. 5. The reason for showing explicitly this one atom region is that it helps to understand the process of cluster growth.

Comparison of Figs. 5(a) and 5(b) shows that, for the atoms in the outer shell, the distance to the second closest atom is, in average, 0.25 a.u. greater than the distance to the first one. The same qualitative behavior is present in the intermediate shell; however, the effect is in this case weaker than before and the values for D_1 and D_2 are more stable, as is clearly indicated by the lower values of the standard deviations. The conclusion is that in this intermediate shell atoms are more homogeneously arranged than in the outer shell.

From Figs. 5(a) and 5(b) we can conclude that, in spite of the overlapping between the standard deviations that is present mainly for the larger aggregates, Cs atoms in finite clusters are closer than in the bulk material and that the atoms in the inner layers are more closely packed than the atoms of the surface. Of course, when cluster size increases it is expected that at least the distances in Figs. 5(a) and 5(b) corresponding to the internal layers should converge to the nearest-neighbor distance in bulk cesium, but what our results show is that this convergence is rather slow and that for $n \leq 100$ we are still far away from the bulk limit, because even for Cs_{78} more than half of the atoms of the cluster are located at its surface. It can be expected that, as the number of atoms in the internal part grows, an expansion toward the bulk distances should occur in the internal regions of the clusters.

B. OCs_n clusters

The results for OCs_n are given in Figs. 6(a) and 6(b) for the two distances D_1 and D_2 corresponding to the three regions in which the aggregates have been divided (see Fig. 2). In this case the strong ionic bonding due to the oxygen impurity gives as a result the very stable and compressed structure of the inner atoms of the clusters, the layer associated with the radius R_2. We shall discuss

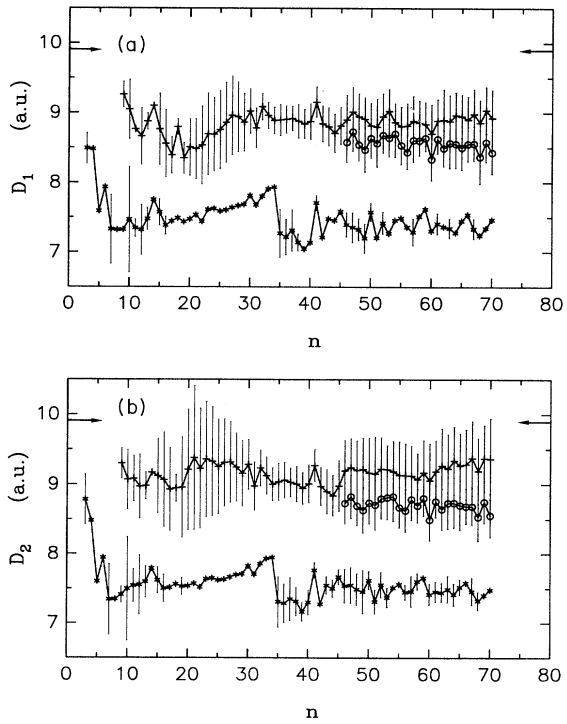

FIG. 6. (a) and (b). The same quantities as in Figs. 5(a) and 5(b), now for the case of OCs_n clusters.

the actual geometrical structures of these regions in the next section. For these clusters only the distances between Cs atoms have been analyzed to obtain D_1 and D_2. All the information about the oxygen-cesium distances was already given in Fig. 2, in particular, the very stable radii of the innermost shells, which are around 5.3 a.u. in the case of octahedral structure, giving a value around 7.5 a.u. for the edge of the octahedron and, consequently, for the values of D_1 and D_2 corresponding to this internal Cs layer. The drop in the values of D_1 and D_2 between OCs_{34} and OCs_{35} is due to the formation of a pentagonal bipyramid, with seven atoms, as the inner structure of the cluster, instead of the octahedron. The former is also the inner shell for OCs_{36} and OCs_{37}, whereas eight atoms forming a square antiprism is the geometry obtained for $n=38$, 39, 40, and 42. The spike in the values of D_1 and D_2 for OCs_{41} is due to the new structure of the internal layer, now formed by nine atoms arranged as a tricapped trigonal prism. Finally, for OCs_{45} a bicapped square antiprism (10 Cs atoms) is the geometry for the inner part before a transition, again to the octahedron, occurs at OCs_{46}. These structures will be also commented in the next section.

The mean values of D_1 and D_2 for the external shell are very similar to those obtained for Cs_n; however, the intermediate shell, for $46 \leq n \leq 70$, shows a contraction which is smaller than the one obtained for the pure case. A very significant overlapping of the standard deviations is present here, indicating the strong dispersion on the values of the distances used to calculate D_1 and D_2 for these two atomic shells. The number of atoms in the intermediate shell and its corresponding mean radii have values that are more stable (independent of n) than those of pure clusters.

The inhomogeneous contraction of the clusters is clearly shown by Figs. 6(a) and 6(b) just by comparing the values of D_1 and D_2 for the outer shells with those of the internal one, the latter being determined by the presence of the oxygen impurity. This influence of the oxygen on the compression of the internal shell is very clear even for those clusters for which the populations of the two atomic layers are identical to those of the pure clusters, $n=26-32$, except $n=29$, as can be seen by comparing Figs. 5 and 6: The values of D_1 and D_2 for the internal shell of these clusters are nearly one atomic unit lower in the case of OCs_n than for the pure clusters. However, the values for the external shell are not very much influenced by the impurity due to the strong screening produced by the inner layer. When D_1 and D_2 for this internal shell are compared with those for the most internal one in pure Cs_n, $64 \leq n \leq 78$, the conclusion can be drawn that the outer shells of the pure cluster produce an effect of compression that is analogous to the one due to the presence of the oxygen atom in the suboxide clusters. Finally, we point again that when the cluster size increases the distances D_1 and D_2 for the internal layers should converge to the bulk distance d_{NN}, except perhaps in the first coordination shell around the oxygen impurity. Our results suggest that the inner structure, in most cases an octahedron, will probably remain stable even in the very large clusters.

V. THE EQUILIBRIUM GEOMETRICAL STRUCTURES

In a previous work[13] we have pointed out that the well-known difficulty of determining the ground-state geometry of an atomic cluster, due to the large number of local minima in the energy hypersurface, is also present in the SAPS method. In fact, from our results we conclude there that the determination of the cluster geometry for a not too small cluster (e.g., Cs_{55}) is a nearly impossible task because of the huge number of local minima. However, many of these minima can be considered as small stable distortions of the ground-state geometry, because of the softness of the aggregates,[22,25] and in that case we expect that the geometry associated with the energy minimum obtained in the SAPS method, starting from a relatively small number of random initial geometries, should be quite close to the true ground-state geometry within our method. This should be especially true for the smaller clusters and for the internal structure of the larger ones for which we present in this section some examples of their geometries. Two effects can be shown from the actual geometries obtained: The complete reconstruction of the pure clusters when they grow in size and also when the oxygen impurity is included in the cluster, and the formation of a compressed inner layer for large clusters.

Our results can be compared with other calculations that avoid the spherical average for the total ionic potential but are restricted to small clusters of light alkaline metals (Na, Li) (see the references quoted in Ref. 22). Unfortunately, direct experimental evidence on the geometrical structures of small clusters is very scarce and difficult to obtain for unsupported aggregates, although information about the actual geometries of the clusters can be extracted from the comparison of the experimental and calculated static electric polarizabilities,[25] which is a measurable property strongly sensitive to the cluster shape. These polarizabilities can be calculated in the SAPS scheme[16] once the geometry is obtained and then compared with the experimental data.

The geometries for Cs_n with $4 \leq n \leq 13$ are identical to those of Na_n calculated by the same method and described in Ref. 22, with the only exception of Cs_8 for which a centered pentagonal bipyramid is obtained instead of the square antiprism of Na_8. Of course, the interatomic distances are different, and we have found that, at least for $n \leq 13$, they are 29–31 % greater than those of Na_n,[22] approximately the same relative variation of the corresponding nearest-neighbor distances of the bulk materials [$d_{NN}(Na)=6.917$ a.u. and $d_{NN}(Cs)=9.896$ a.u.]. Summarizing, the calculated geometries of Cs_n are the following: tetrahedron, $n=4$; trigonal bipyramid, $n=5$; octahedron, $n=6$; centered octahedron (O_h), $n=7$; centered square antiprism (C_{4v}), $n=9$; centered tricapped trigonal prism (D_{3h}), $n=10$; centered square antiprism bicapped at the square faces (C_{4v}), $n=11$; distorted and centered icosahedron with one vertex lost, $n=12$, and a perfect centered icosahedron for $n=13$ with a value for its edge of 9.9 ± 0.1 a.u. The structures for Cs_{10} and Cs_{11} are given in Fig. 7, together with those of larger clusters

that present relevant properties of symmetry. Also, the corresponding geometries for OCs_n are given for comparison. Cs_{15} is a bicapped hexagonal antiprism with a central atom, Cs_{16} has a D_{3h} symmetry and can be described as a centered trigonal prism with two atoms over each rectangular face and one more centered over each of the long edges of these faces, Cs_{18} is a centered pentagonal prism capped in all its faces preserving a fivefold symmetry, and Cs_{19} is the first cluster with two atoms in the inner part, its external structure being identical to the one of Cs_{18}. Finally, Cs_{20} is given in Fig. 8 and its remarkable geometry (D_{3h}) is completely different from the one obtained for Na_{20},[22] in which only two atoms are located inside the structure. A visualization of the effect of shrinking can be obtained from this last cluster by comparing the mean values of the edges of the inner and the outer polyhedra. An internal tetrahedral structure is also obtained for Cs_n with $n=21-25$, and an octahedral one is formed in the inner region for $n=26-32$ with the only exception of $n=29$.

For the suboxide clusters OCs_n the geometries of the

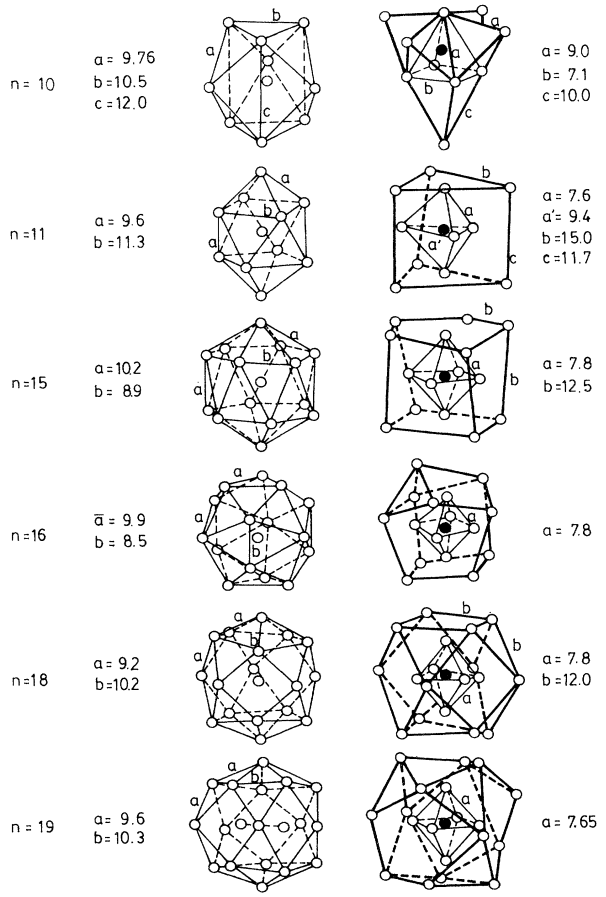

FIG. 7. Equilibrium geometries for Cs_n (left-hand column) and OCs_n (right-hand column) for $n=10$, 11, 15, 16, 18, and 19. Open and solid circles correspond to Cs and O atoms, respectively. For Cs_{19} the two internal atoms are linked by a line. The indicated distances are in atomic units.

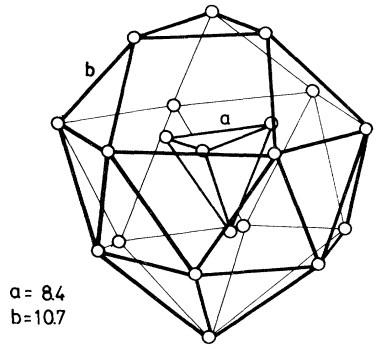

FIG. 8. Equilibrium geometry for Cs_{20}. The distances are in atomic units.

Cs cover are completely modified by the presence of the O atom, except in those light clusters for which the central site is empty ($n=4,5,6$). The presence of the oxygen atom produces a general contraction of the clusters, for example, the edge of the octahedron changes from 9.52 a.u. in the pure case to 7.96 a.u. for OCs_6, indicating again the strong ionic bonding between the impurity and the Cs atoms. This contraction is also present for those Cs_n clusters with their internal layer formed by six atoms, as we have mentioned in Sec. III and was shown in Fig. 4. For the other clusters we obtain pentagonal bipyramid, $n=7$; square antiprism, $n=8$; tricapped trigonal prism, $n=9$ (this is the first cluster with two separated atomic layers, of six and three atoms, respectively, and its geometry is given in Fig. 9). The geometries for OCs_{10} and OCs_{11} are given in Fig. 7, where it is seen that the inner Cs layer has five atoms for both clusters but the corresponding structures are completely different (a square pyramid and a trigonal bipyramid, respectively) and the outer atoms can be considered as coordinated to each of the faces of those internal structures. OCs_{12} has also a trigonal bipyramid as internal geometry, but for $13 \le n \le 34$ and $46 \le n \le 70$ the internal structure is always an octahedron with the only exception being OCs_{61}, for which a trigonal bipyramid is obtained. The structure of OCs_{14} was already given in Ref. 13: an octahedron with one Cs atom coordinated to each one of its eight

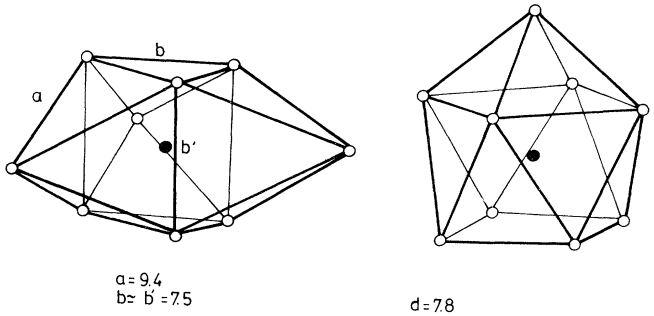

FIG. 9. The structure of OCs_9 (left) and of the internal region of OCs_{44}, both formed by nine Cs atoms surrounding the O atom. The symbols and distances are as in Fig. 7. (d) is the mean value of the plotted edges.

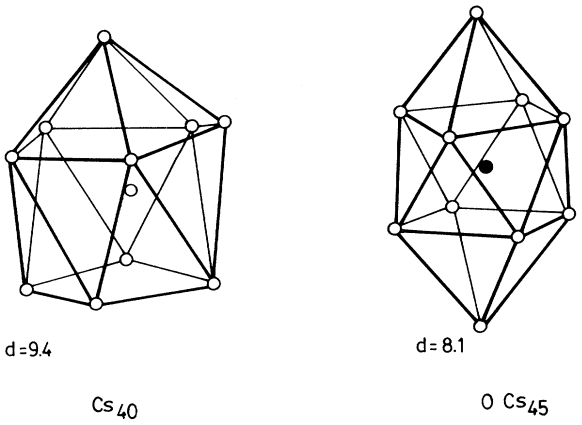

FIG. 10. The structures of the internal layer for Cs_{40} (left) and OCs_{45} (right). The values of (d) are as in Fig. 9.

faces (O_h), and those for $n=15$, 16, 18, and 19 are plotted in Fig. 7. Particularly notorious is the distorted cuboctahedron for OCs_{18} which surrounds the inner octahedron, preserving the global O_h symmetry.

Some of the structures for the internal layers with a low number of atoms are given in Figs. 9–11 to show that our method is able to describe the influence of the external shells on the inner structure producing geometries different from those of the single layered clusters. In Fig. 9, OCs_9 and the nine Cs atoms of the inner shell of OCs_{44} are compared, showing a completely different geometry. Also, the internal shell of OCs_{41} is formed by nine atoms surrounding the oxygen, with a structure identical to that of OCs_9 but with different values for the distances quoted in Fig. 9(a). These are now the following: $a=7.8$ a.u., $b\simeq a$, and $b'=8.6$ a.u., indicating that the presence of the outer shell of Cs atoms produces a contraction of the radial distances of the atoms in the inner region of the cluster. Figure 10 gives the case of Cs_{40} and OCs_{45}, both with 10 atoms surrounding the central one, which can be compared with Cs_{11} and OCs_{10} in Fig. 7; it is clear that the equilibrium geometries are determined by the actual environment of the clusters and that there is a complete reconstruction of the aggregate when the total number of atoms is modified. Two more examples of centered internal structures are given in Fig. 11 for Cs_{46} and Cs_{53} because of its symmetry properties. For $n=46$, 12 atoms are arranged around the central one in a form which is different from the icosahedron of Cs_{13} or from the cuboctahedron. The structure of 15 atoms corresponding to Cs_{53} is a distorted cuboctahedron bicapped on its square faces and with a central atom, a structure which is different from the one obtained for pure Cs_{15} given in Fig. 7, showing again the influence of the external Cs atoms in the equilibrium geometries of the internal layer.

VI. SUMMARY

The geometrical structures found in our calculations indicate that atoms in the clusters are arranged in spherical layers around the cluster center and that those geometries for which no atom has its closest neighbor at a distance clearly greater than d_{NN} (bulk nearest neighbor) are preferred as equilibrium geometries. The ionic bonding of the oxygen impurity strongly modifies the structural arrangement of Cs_n clusters and, on the other side, it produces a stable inner structure (mostly an octahedron) around which the rest of the Cs atoms are located, also in spherical layers. In the growing of this external part the formation of a new intermediate shell seems to be ruled by the same condition as for pure clusters: no closest neighbor at a distance greater than d_{NN}.

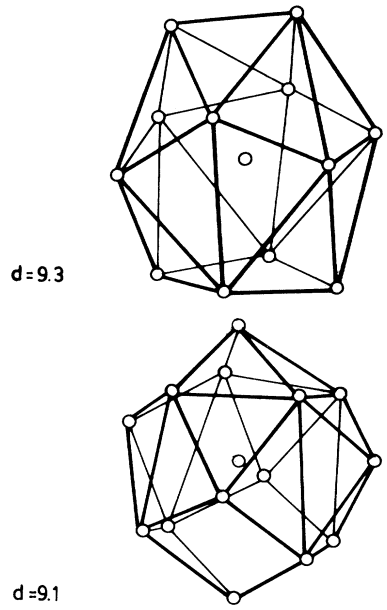

FIG. 11. The structures of the internal layer for Cs_{46} (upper) and Cs_{53} (lower). The values of (d) are as in Fig. 9.

The geometrical arrangement of the aggregates in atomic spherical layers allows for the analysis of the interatomic distances for atoms located at different regions of the clusters. When the distances from one atom to its two closest atoms are considered, the values obtained show that the atoms in the inner parts of the clusters are more densely packed than those on the outer parts. This effect should be related to the fact that, for the size range studied, more than half of the atoms of the aggregates are located at the surface and then the strong surface tension produces the shrinking of the cluster, and what is remarkable is that, according to our calculations, it is an inhomogeneous one. It should be interesting to check these conclusions for other simple metal clusters.

ACKNOWLEDGMENTS

This work has been supported by Dirección General de Investigación Científica y Técnica of Spain (Grant Nos. PB 86-0654-C02-01 and PB 89-0352-C02-01) and by NATO.

[1]Proceedings of ISSPIC-4, Aix-en-Provence, 1988, edited by C. Chapon, M. F. Gillet, C. R. Henry [Z. Phys. D **12**, (1989)].
[2]W. A. De Heer, W. D. Knight, M. Y. Chou, and M. L. Cohen, Solid State Phys. **40**, 93 (1987).
[3]W. D. Knight, K. Clemenger, W. A. De Heer, W. A. Saunders, M. Y. Chou, and M. L. Cohen, Phys. Rev. Lett. **52**, 2141 (1984).
[4]W. Ekardt, Phys. Rev. B **29**, 1558 (1984).
[5]W. A. Saunders, K. Clemenger, W. A. De Heer, and W. D. Knight, Phys. Rev. B **32**, 1366 (1985).
[6]Z. Penzar and W. Ekardt, Z. Phys. D **17**, 69 (1990).
[7]A. Rubio, L. C. Balbás, and J. A. Alonso, in Proceedings of ISSPIC-5, Konstanz, 1990, edited by O. Echt and E. Recknagel [Z. Phys. D **19**, 93 (1991)].
[8]H. Göhlich, T. Lange, T. Bergmann, and T. P. Martin, Phys. Rev. Lett. **65**, 748 (1990).
[9]T. Lange, H. Göhlich, T. Bergmann, and T.P. Martin, in Proceedings of ISSPIC-5, Konstanz, 1990, edited by O. Echt and E. Recknagel [Z. Phys. D. **19**, 113 (1991)].
[10]T. P. Martin, T. Bergmann, H. Göhlich, and T. Lange, Chem. Phys. Lett. **172**, 209 (1990).
[11]M. P. Iñiguez, M. J. López, J. A. Alonso, and J. M. Soler, Z. Phys. D **13**, 171 (1989).
[12]U. Lammers, A. Mañanes, G. Borstel, and J. A. Alonso, Solid State Commun. **71**, 591 (1989).
[13]U. Lammers, G. Borstel, A. Mañanes, and J. A. Alonso, Z. Phys. D **17**, 203 (1990).
[14]H. G. Limberger and T. P. Martin, Phys. Rev. Lett. **60**, 1767 (1988).
[15]T. Bergmann, H. G. Limberger, and T. P. Martin, Phys. Rev. Lett. **60**, 1767 (1988).
[16]A. Rubio, L. C. Balbás, and J. A. Alonso, Solid State Commun. **75**, 139 (1990).
[17]C. Solliard and M. Flueli, Surf. Sci. **156**, 478 (1985).
[18]P. A. Montano, W. Schulze, B. Tesche, G. K. Shenoy, and T. I. Morrison, Phys. Rev. B **30**, 672 (1984).
[19]P. A. Montano, G. K. Shenoy, E. E. Alp, W. Schulze, and J. Urban, Phys. Rev. Lett. **56**, 2076 (1986).
[20]J. Robles, M. P. Iñiguez, J. A. Alonso, and A. Mañanes, Z. Phys. D **13**, 269 (1989).
[21]R. G. Parr and W. Yang, *Density Functional Theory of Atoms and Molecules* (Oxford University Press, New York, 1989).
[22]A. Mañanes, M. P. Iñiguez, M. J. López, and J. A. Alonso, Phys. Rev. B **42**, 5000 (1990).
[23]P. Ballone, W. Andreoni, R. Car, and M. Parrinello, Europhys. Lett. **8**, 73 (1989).
[24]M. J. López, M. P. Iñiguez, and J. A. Alonso, in Proceedings of ISSPIC-5, Konstanz, 1990, edited by O. Echt and E. Recknagel [Z. Phys. D **19**, 141 (1991)].
[25]I. Moullet, J. L. Martins, F. Reuse, and J. Buttet, Phys. Rev. Lett. **65**, 476 (1990); Phys. Rev. B **42**, 11 598 (1990).